Cellulose (2023) 30:9501–9515
https://doi.org/10.1007/s10570-023-05417-z

ORIGINAL RESEARCH

Highly hydrophobic cellulose acetate mats modified with poly(ethylene oxide-b-propylene oxide-b-ethylene oxide) triblock copolymer and TiO_2 nanoparticles by electrospinning

Joseba Gomez-Hermoso-de-Mendoza · Junkal Gutierrez · Agnieszka Tercjak

Received: 30 November 2022 / Accepted: 19 July 2023 / Published online: 29 July 2023

Abstract Cellulose acetate (CA) mats modified with poly(ethylene oxide-b-propylene oxide-b-ethylene oxide) (PEO-b-PPO-b-PEO or EPE) and sol–gel synthesised titanium oxide (TiO_2) nanoparticles were successfully fabricated by using electrospinning technique. Under the same preparation conditions, higher spinnability was achieved for EPE triblock copolymers modified mats. All fabricated mats showed a micrometric multilayer structure, which enabled layer-by-layer peeling. The addition of TiO_2 nanoparticles facilitated the peeling process. The diameter of the fibres was ~3 times lower after the incorporation of sol–gel synthesised TiO_2 nanoparticles. TEM images confirmed that under electrospinning conditions the PPO block domains were able to microphase separated from the PEO block/CA phase. Additionally, the introduction of sol–gel synthesised TiO_2 nanoparticles led to an inorganic network formation with nanoparticle size equal to ~8 nm in diameter. Moreover, the addition of TiO_2 nanoparticles increased the hydrophobicity of the mats and their self-cleaning ability, being more effective for TiO_2/CA than for TiO_2-EPE/CA due to the partial absorption of water by EPE triblock copolymer. Young's modulus of fabricated mats improved drastically with the addition of TiO_2 nanoparticles, as well as their physical integrity in polar and nonpolar solvents. Fabricated mats with enhanced spinnability, which maintain CA mat features as well as the properties associated with sol–gel synthesised TiO_2 nanoparticles, can find a wide range of applications.

Keywords Electrospinning · Polymer fibres · TiO_2 nanoparticles · Hydrophobic materials · Self-cleaning

Introduction

Electrospinning is a highly versatile and widely used technique employed in the preparation of micro and nano polymer fibres with tuneable properties such as high porosity and high specific surface area (Li and Yang 2020; Wable et al. 2021).

This technique consists of injecting the polymer solution through a syringe, applying an electric potential difference between the needle and the fibre collector, which can be stationary or rotating (Luraghi et al. 2021). The spinnability of the fibres

Supplementary Information The online version contains supplementary material available at https://doi.org/10.1007/s10570-023-05417-z.

J. Gomez-Hermoso-de-Mendoza · J. Gutierrez (✉) · A. Tercjak (✉)
Group 'Materials+Technologies' (GMT), Department of Chemical and Environmental Engineering, Faculty of Engineering Gipuzkoa, University of the Basque Country (UPV/EHU), Plaza Europa 1, 20018 Donostia-San Sebastian, Spain
e-mail: juncal.gutierrez@ehu.eus

A. Tercjak
e-mail: agnieszka.tercjaks@ehu.eus

can be modified varying the different technique parameters, such as the applied voltage, the distance between the needle tip and the collector, the polymer concentration in the solution and the polymer feed rate (Angel et al. 2020), which affect their final morphology and properties.

Moreover, the spinnability can be improved by adding low contents of additives, such as poly(ethylene oxide) (PEO) (Li and Yang 2020; Santamaria-Echart et al. 2017). Thus, taking into account the possibilities offered by electrospinning, the polymer mats fabricated by this technique show promising utility as biosensor-integrated drug delivery systems, and membrane-based systems for tissue engineering, among others (Cai et al. 2016; Yoon et al. 2009).

The preparation of hybrid inorganic/organic polymeric materials via the electrospinning technique is a fast-growing field of research (Angel et al. 2022; Rodríguez-Tobías et al. 2019; Vahabi et al. 2021) due to the possible applications they can offer, from piezoelectric materials (Chamankar et al. 2020; Mimura et al. 2010) to materials with improved antibacterial properties (Chong et al. 2022; Morselli et al. 2017).

Moreover, electrospun fibres with TiO_2 nanoparticles (Gosal et al. 2019) were studied owing to their high thermal and chemical stability, and good optical properties (Zhang et al. 2018), by employing commercial titanium dioxide (TiO_2) nanoparticles with different polymeric matrices such as poly(lactic acid) (PLA) (Toniatto et al. 2017), polycaprolactone (PCL) (Nandagopal et al. 2016), PEO (de la Cruz et al. 2016) and polystyrene (PS) (Neppalli et al. 2014), while also by employing the sol–gel synthesised TiO_2 method with poly(vinyl alcohol) (PVA) (El-Aassar et al. 2016) and polyvinylpyrrolidone (PVP) (Passaro et al. 2022).

Attractive features of cellulose acetate (CA) such as biodegradability, low cost, high availability and good biocompatibility (Gorbacheva et al. 2021; Zhou et al. 2021) ensure its utilization as an electrospun matrix for different nanocomposites, especially for the development of membranes. In this context, Goetz et al. (2016) achieved CA electrospun mats impregnated with chitin nanocrystals (ChNC) for water filtration membranes with improved mechanical properties, lower biofouling and high hydrophilic character. Membranes for photodegradation of organic dyes [rhodamine B (RhB), methylene orange (MO) and methylene blue (MB)] were also prepared using recycled cellulose triacetate (rTAC) modified with commercial graphene and synthesised TiO_2 and silver vanadate (Ag_3VO_4) nanoparticles (Motora et al. 2020). In the same way, Tian et al. (2015) and Nair and Mathew (2017) fabricated CA membranes with commercial hydroxyapatite (HAp) and cellulose nanocrystal (CNC) for Bovine serum albumin (BSA) and Victoria Blue adsorption, respectively. Besides their use as membranes, CA electrospun nanocomposites were also employed for biomedical applications after being modified with commercial ferric oxide (Fe_2O_3) nanoparticles (Tsioptsiasa et al. 2010), silk fibroin, silver (Ag) and gold (Au) nanoparticles (Arumugam et al. 2021), among others.

The improvement of the mechanical properties is essential for the development of competitive electrospun materials. In this regard, Wang et al. (2020) achieved significant improvement in the Young's modulus (13%) and the tensile strength (11%) for CA-PAN (polyacrylonitrile) polymer blend with 33 wt% of CA, if compared with the mechanical properties of neat PAN mat. Similarly, Arrieta et al. (2020) improved by ~ 20% the elongation at break of PLA/PHB (poly(lactic acid)/polyhydroxybutyrate) blends adding 15% of oligomeric lactic acid (OLA), without affecting the Young's modulus. These sustainable flexible blends are good candidates to be used in agricultural applications. In the case of nanocomposites, the addition of 1% of graphene nanoplatelets (GNP) drastically increased the tensile strength (229%) and elongation at break (131%) of chitosan/PVA blends (Bazzi et al. 2022). Furthermore, the introduction of 1.5% of graphene oxide (GO) increased the Young's modulus and tensile strength of CA up to 75% and 73%, respectively (Aboamera et al. 2019).

In this study, the cellulose acetate based mats modified with poly(ethylene oxide-b-propylene oxide-b-ethylene oxide) triblock copolymer and sol–gel synthesised TiO_2 nanoparticles were fabricated by the electrospinning technique. This investigation work was done to verify the hypothesis that the addition of EPE block copolymer increased the spinnability of cellulose acetate (CA). Moreover, the preparation of nanocomposite based on CA or CA/EPE with sol–gel synthesized TiO_2 nanoparticles by using the electrospinning process was proved with the aim to

enhance the mechanical properties of CA membranes. The thermal and morphological properties of the prepared mats were deeply studied. Moreover, the wettability was investigated by the water contact angle, and mats were immersed in different solvent to study their solvent resistance. In addition, the self-cleaning properties of the mats were also analysed.

Experimental section

Materials

Cellulose acetate (CA, Mn 50,000 g mol^{-1}, DS = 2.5), poly(ethylene oxide-b-propylene oxide-b-ethylene oxide) triblock copolymer (PEO-b-PPO-b-PEO or EPE, Mn 12,600 g mol^{-1}, 70 wt% PEO) and titanium (IV) isopropoxide ($Ti[OCH(CH_3)_2]_4$) (TTIP) were supplied by Sigma Aldrich. Toluene and hydrochloric acid (37%) were purchased from Scharlau and isopropanol (IPA) from Panreac. All the reagents were the analytical grade and were used as received.

Preparation of mats

Solutions of CA and EPE/CA (20:80 weight ratio) were prepared in acetone, maintaining a total concentration of 12.5 wt%. On the other hand, IPA, toluene and TTIP were mixed (7:7:1 volume ratio), acidifying the solution with hydrochloric acid (approx. pH 2), to prepare the titanium sol–gel solution. This mixture was stirred for 1 h. After that, 40 vol% sol–gel solution was incorporated to CA or EPE/CA solution to obtain TiO_2/CA or TiO_2-EPE/CA solutions, respectively, and finally were kept stirring 1 h more.

FLUIDNATEK LE-10 electrospinning machine from Bionicia was employed to spin prepared solutions at ambient conditions, using a blunt needle tip (Model: 21G Sterican, B Braun) of 0.8 mm diameter and 22 mm length. Feed rate was kept constant at 4 mL h^{-1} and the distance between the needle tip and the stationary collector was fixed at 7 cm. The voltage applied on the needle was equal to 9 kV, while the stationary collector voltage was −0.8 kV. Fabricated mats were collected on the surface of aluminium foil (20 cm × 20 cm) and electrospinning was carried out during 5 h for CA and EPE/CA, and 8 h for TiO_2/CA and TiO_2-EPE/CA, in order to ensure a similar weight (~2 g) of the prepared CA and EPE/CA mats. The thickness of developed mats was ~0.15 mm for CA and EPE/CA mats and ~0.50 mm for TiO_2/CA or TiO_2-EPE/CA mats.

Characterisation

Mettler Toledo DSC3+ was employed to carry out differential scanning calorimetry (DSC) measurements. Sealed aluminium pans containing a mat weight of 2–3 mg were used. Scans were performed at a heating rate of 20 °C min^{-1} and under N_2 atmosphere. Pans were stabilized at 0 °C for 10 min, then heating to 250 °C, followed by a cooling to 0 °C and subsequent stabilized for 10 min, and finally heating to 250 °C. The second heating was plotted in order to avoid the thermal history of investigated mats. The degree of crystallinity of CA phase and PEO block was calculated with the following equation, with the value of the melting enthalpy of 100% crystalline CA (Cerqueira et al. 2006) and PEO (Zheng et al. 2003).

$$X_{c,i} = \frac{\Delta H_{m,i}}{w_i \cdot \Delta H^{\circ}_{m,i}} \cdot 100$$

where $X_{c,i}$ is the degree of crystallinity of component i, $\Delta H_{m,i}$ is the melting enthalpy of component i, w_i is the weight fraction of component i and ΔH°_{m} is the melting enthalpy of 100% crystalline component i.

Thermogravimetric analysis (TGA) were performed in a Mettler Toledo TGA/DSC3+ equipment, from 25 to 900 °C under air atmosphere at a 10 °C min^{-1} heating rate, with a sample weight of ~3 mg.

Scanning electron microscope (SEM) images (surface and cross-section) were collected using a Hitachi S-4800. Fibre mats were analysed with an accelerating voltage of 5 kV. Investigated mats were cut using liquid nitrogen. The ImageJ software programme was used in order to measure the size of the fibres and the pores of each fabricated mat. The average diameter of each entity was calculated by analysing around 20–25 randomly selected fibres or pores using for this purpose 3 different SEM images.

Mechanical test specimens were cut with a dog-bone shape with a pneumatic sample cutting press

(Metrotec) according to ASTM D 1708-02 standard and conditioned for 48 h under vacuum prior to testing. The mechanical properties were evaluated at room temperature on an Instron 5967 testing machine, with a load cell of 50 N and a strain rate of 3 mm min^{-1}. The length between grips was set at 18 mm. The Young's modulus was calculated as an average out of five test specimen data.

The water contact angle (WCA) was studied with DataPhysics contact angle system (Model OCA 20), repeating the measurements six times for each mat.

Self-cleaning experiments were carried out fixing a square piece of developed mat in a glass plate, placing it with a 13° inclination, following the procedure describe elsewhere (Wang et al. 2022a, 2022b). Pink chalk powder was deposited on the surface of each investigated mat and removed with 1 mL of water. The surface of each mat was studied by optical microscopy (OM), Nikon Eclipse 80i in transmission mode, before and after the self-cleaning process.

Solvent resistance of the fabricated mats was also studied immersing in distilled water, IPA, acetone and toluene for 7 days, weighting them before and after that time.

Mats were also characterized by a colorimeter and transmission electron microscopy (TEM). Details are given in the Supplementary Material.

Results and discussion

Appearance of fabricated mats

CA and EPE/CA mats displayed very similar appearance and colour, without any significant differences (Fig. 1). Both mats presented L*, a* and b* colour parameters according to their white colour (Table S1 of Supplementary Material). The addition of sol–gel synthesised TiO_2 nanoparticles into these mats resulted in slight increase of the L* value and as a consequence of ΔE*, which is attributed to the bleaching effect of TiO_2 nanoparticles (Cao et al. 2022; El-Aassar et al. 2016).

Deeper analysis of the investigated mats allowed to distinguish a micrometric multilayer structure for all of them, especially visible for TiO_2/CA and TiO_2-EPE/CA mats, as clearly shown in the digital images and cross-section SEM images in Fig. S1 of the Supplementary Material. The electrospinning process and the employed conditions led to mats being

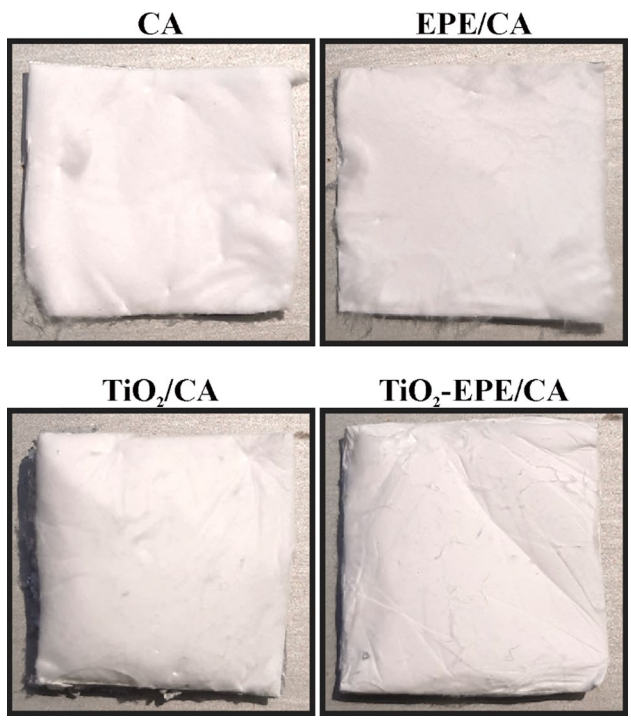

Fig. 1 Digital images of fabricated mats (2 cm × 2 cm)

organised into successive micrometric layers, which can be removed individually from each fabricated mat and the incorporation of TiO_2 nanoparticles promoted this structure. The thickness of each individual layer was ~0.04 mm for all the mats.

Thermal behaviour and stability

Figure 2 shows DSC thermograms and TGA curves of fabricated mats. CA mat showed a T_g and T_m at 193 and 228 °C, respectively, and a degree of crystallinity equal to 2.6% (Table S2). After the addition of EPE triblock copolymer, the T_g decreased to 187 °C and the T_m to 223 °C, indicating the partial miscibility of PEO block of EPE triblock copolymer and CA through the formation of intermolecular hydrogen bonds between the hydroxyl groups of CA and the ether oxygen of PEO blocks (Gutierrez et al. 2017). Moreover, the T_m of PEO block appeared at 53 °C, with a degree of crystallinity of ~13%.

For TiO_2/CA mat, the T_g of CA phase shifted 5 °C to a lower temperature if compared to the T_g of CA mat. Furthermore, the melting enthalpy was difficult to calculate, which was indicative of the low degree of crystallinity of CA phase of TiO_2/CA mat. Therefore, the CA was compatible with the TiO_2 nanoparticles, most likely due to the formation of hydrogen bonds between the hydroxyl groups of sol–gel nanoparticles and the ether or carbonyl group of CA. The possible hydrogen bond formation was study by FTIR. FTIR spectra of fabricated mats are showed in Fig. S2 of Supplementary Material. The addition of sol–gel synthesised TiO_2 nanoparticles into CA and EPE/CA mats resulted in

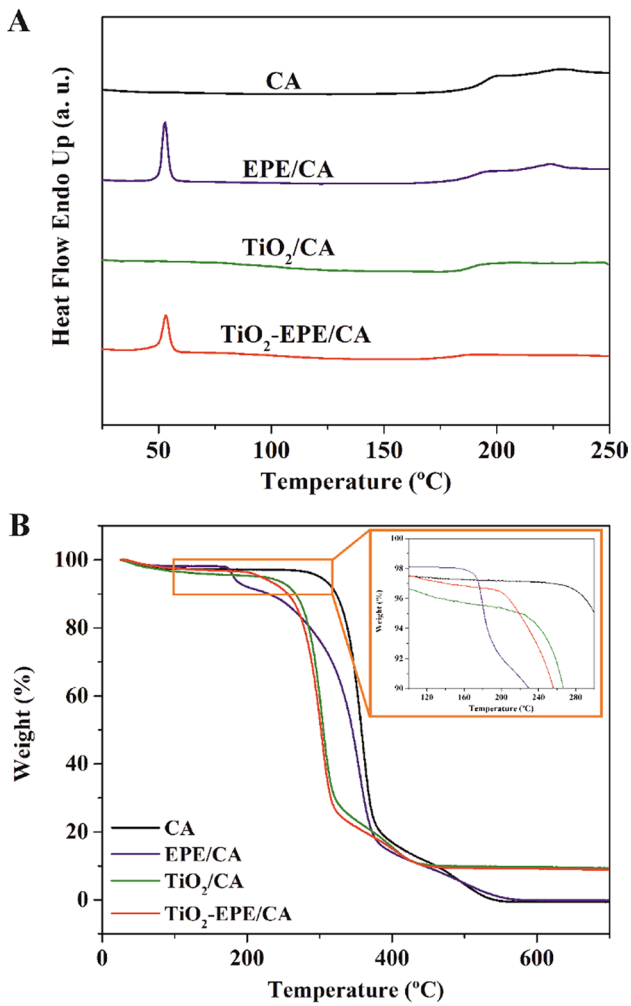

Fig. 2 **A** DSC thermograms and **B** TGA curves of fabricated mats (zoom in the range of 100–300 °C is shown as inset)

a slight displacement of –OH stretching band region to lower wavenumbers and peaks became broader confirming hydrogen bond formation.

For TiO_2-EPE/CA mat, the T_g of CA phase appeared at 14 °C, which is a lower temperature if compared with the T_g of CA mat and 8 °C if compared with EPE/CA mat.

This behaviour confirmed that incorporated sol–gel synthesised TiO_2 nanoparticles were compatible not only with CA but also with PEO block of EPE triblock copolymer. The T_m of PEO block remained at 53 °C, however the degree of crystallinity decreased to ~ 11% if compared with EPE/CA mat, which was in accordance with the above mentioned compatibility.

As for the thermal stability, CA mat showed a three-step thermal degradation process (Fig. 2B) (Gutierrez et al. 2013). The first one, a minor decrease ~ 100 °C, was ascribed to the evaporation of the water adsorbed from the environment. The second (270–420 °C) and the third (440–560 °C) weight loss corresponded to the degradation of CA (mainly dehydration and decarboxylation reactions) and the degradation of generated char (Gaan et al. 2009; Gutierrez et al. 2012). For EPE/CA mat, the second weight loss started at lower temperatures if compared with CA mat, at around 220 °C. Moreover, a weight loss around 180 °C was detected, corresponding to the degradation of EPE triblock copolymer (Gomez-Hermoso-de-Mendoza et al. 2019).

In the case of TiO_2/CA and TiO_2-EPE/CA mats, the second and third degradation steps occurred at slightly lower temperatures if compared with CA mat (220–360 °C for second and 370–470 °C for third one), indicating the considerable lower thermal stability of mats modified with sol–gel synthesised TiO_2 nanoparticles. This behaviour was also reported in the literature and can be attributed to the presence of traces of remaining water, isopropanol and the unreacted isopropoxide groups in formed sol–gel TiO_2 nanoparticle network (Gutierrez et al. 2013; Zeng et al. 2010). For TiO_2-EPE/CA mat, a slight decrease can be observed at 190 °C corresponding to the degradation of EPE triblock copolymer (Fig. 2B zoom inset).

Furthermore, the remaining final inorganic residue confirmed that the content of TiO_2 nanoparticles was 10 wt% for both mats with this being indicative of the reproducibility of the preparation protocol.

Despite the differences observed in the degradation steps, it can be concluded that the addition of EPE and sol–gel synthesised TiO_2 nanoparticles did not significantly affect the thermal stability of mats and can be used in the same temperature range as CA mat.

Morphology

Figure 3 shows the surface morphologies of CA based mats investigated by SEM. First of all, it should be mentioned that all investigated CA based mats presented uniformly distributed, smooth on the surface fibres clearly visualized in higher magnification SEM images.

These higher magnification SEM images affirmed also the lack of both the macrophase separation of PPO block of EPE triblock copolymer for EPE/CA mat and the sol–gel synthesised TiO_2 nanoparticles agglomerations for TiO_2/CA and TiO_2-EPE/CA mats. The fibres of CA mat (Fig. 3A) were randomly oriented with a diameter size of 5.2 ± 1.3 µm (Fig. S3). This mat consisted of homogeneously distributed fibres with very few visible beads, and with highly smooth surfaces. Moreover, the pore size was 2.4 ± 1.1 µm for this mat (Fig. S3). EPE/CA mat had very similar distribution (Fig. 3B) and fibres diameter (3.8 ± 1.7 µm), as well as similar pore size (3.2 ± 1.3 µm). However, here it should be pointed out that a better spinnability was achieved for this mat if compared with CA.

This is ascribed to the addition of EPE triblock copolymer with high PEO block content since, as is well known from the literature (Li and Yang 2020; Santamaria-Echart et al. 2017), PEO homopolymer can enable the electrospinning process.

In the case of TiO_2/CA and TiO_2-EPE/CA mats, the fibres presented higher stretching and as a consequence lower diameter if compared with fibres of CA and EPE/CA mats. This is due to the addition of sol–gel solution, which provoked a dilution of CA or EPE/CA solutions, which decrease the amount of electrospun mass per minute. The diameter of the fibres was 1.8 ± 0.6 µm for TiO_2/CA and 1.4 ± 0.4 µm for TiO_2-EPE/CA, indicating higher fibres diameter uniformity of mats without sol–gel synthesised TiO_2 nanoparticles.

Moreover, the smaller diameter of the fibres led to a larger number of fibres per unit area, therefore the density of these mats seems to be higher than those

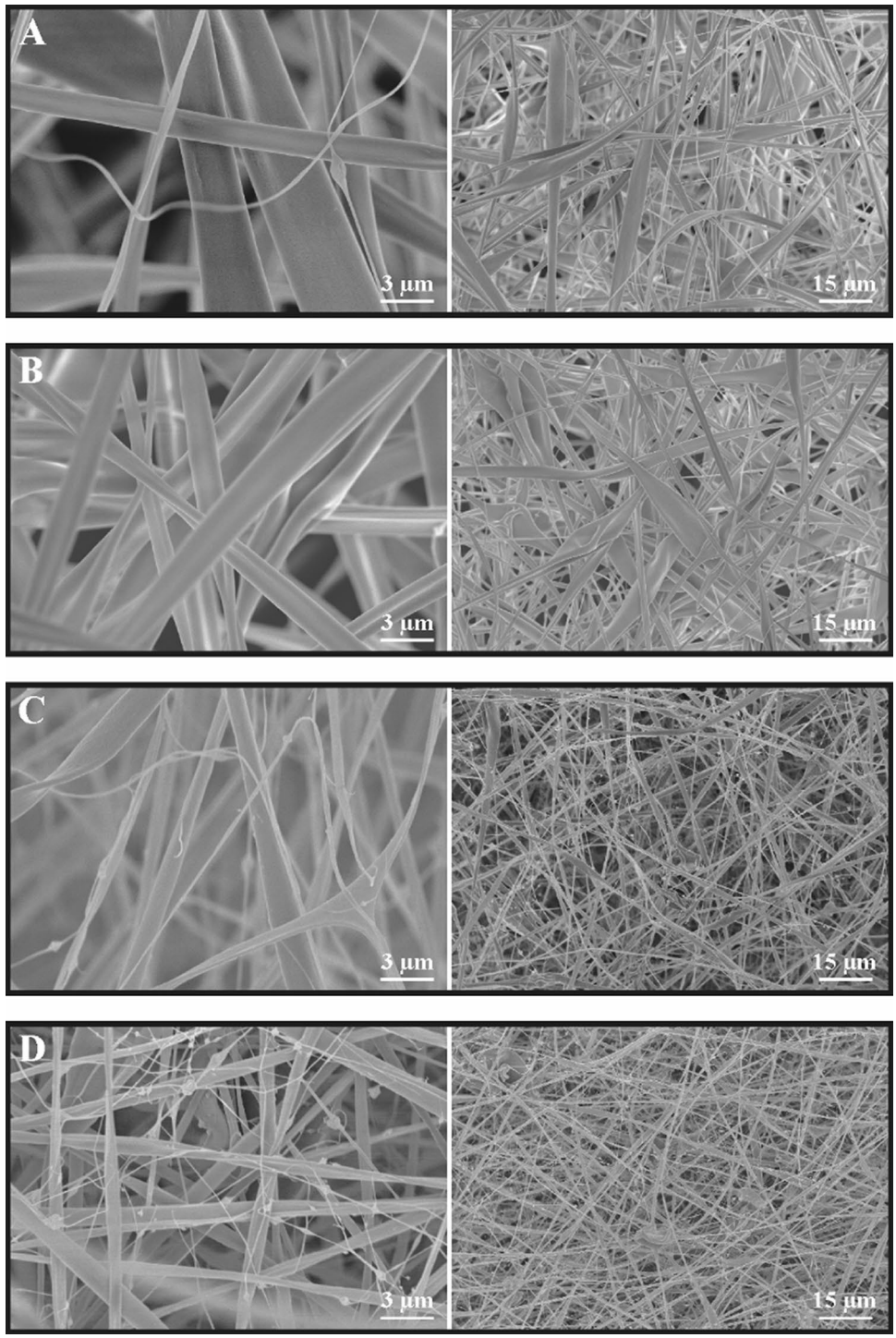

Fig. 3 SEM images of fabricated mats at different magnifications: **A** CA, **B** EPE/CA, **C** TiO_2/CA and **D** TiO_2-EPE/CA

without TiO_2 nanoparticles. As a consequence, the pore size was lower for mats with sol–gel synthesised TiO_2 nanoparticles (1.2 ± 0.4 µm for TiO_2/CA and 0.9 ± 0.4 µm for TiO_2-EPE/CA) if compared with CA and EPE/CA mats. As for the bead formation, in both cases some small beads were detected, with a size of 0.7 ± 0.2 µm. However, these beads did not affect mat formation and fibre morphology. As in case of EPE/CA mat, the electrospinning process was more efficient for TiO_2-EPE/CA mat than for TiO_2/CA as a consequence of the addition of PEO block of EPE triblock copolymer.

In order to study more deeply the morphology of fabricated mats, TEM measurement were performed. CA and EPE/CA fibres (Fig. S4A and B of Supplementary Material) displayed smooth surfaces whereas for EPE/CA some black circular (~14 nm) and worm-like domains (~50 nm) were detected (marked in white in Fig. S4B). These microseparated domains could correspond to PPO block phase separated from the PEO block/CA phase (Gomez-Hermoso-de-Mendoza et al. 2021). Only a few domains were detected on the analysed surface of the fibres due to the low amount of PPO block in the mat (~6 wt%).

On the other hand, the surface of fibres completely changed to mopped surface when sol–gel solution was added (Figure S3C and D). This can be easier distinguished if compared to TEM images of mats without and with sol–gel synthesised TiO_2 nanoparticles (CA mat with TiO_2/CA mat and EPE/CA mat with TiO_2-EPE/CA mat). Small in diameter (~8 nm) and almost interconnected between each other, TiO_2 nanoparticles were well-dispersed along the fabricated fibres. Moreover, the fibres maintained their smooth surface, in which no apparent modification of their surface was observed. For TiO_2-EPE/CA mat some PPO block domains (white circles) were also detected as for EPE/CA mat, which indicated that the microphase separation of the PEO block of EPE triblock copolymer took place even in the presence of TiO_2 nanoparticles.

Table 1 Young's modulus of fabricated mats

Sample	Young's modulus (MPa)
CA	7.07 ± 2.50
EPE/CA	1.49 ± 0.51
TiO_2/CA	82.60 ± 10.30
TiO_2-EPE/CA	78.45 ± 8.97

Mechanical properties

The Young's modulus of CA mat was ~7 MPa (Table 1), slightly higher if compared with the values of electrospun cellulose acetate mats previously published elsewhere (Ghorani et al. 2013; Sinha et al. 2020; Wang et al. 2020), with values between 1 and 3 MPa. The electrospinning conditions affects fibre diameter, mat porosity and bead formation, among others (Angel et al. 2020; Can-Herrera et al. 2021), which have a strong impact on the mechanical properties. Thus, the conditions employed in this work led to mats with improved stiffness. After the incorporation of EPE triblock copolymer, the Young's modulus decreased to 1.5 MPa due to the plasticising effect of PEO block of EPE.

TiO_2/CA mat showed a drastic increase of the Young's modulus (from 7 to 83 MPa, 12 times higher) if compared with CA mat that implies a significant increment in the stiffness of this mat. This phenomenon can be correlated with the reinforcement effect of sol–gel synthesised TiO_2 nanoparticles (Zhang et al. 2022). It can be also appreciated in their handling, since mats with sol–gel synthesised TiO_2 nanoparticles were stronger to touch. This increase was also high for TiO_2-EPE/CA mat, with a value of ~78 MPa if compared to 1.5 MPa of EPE/CA mat, that is, 52 times higher. Therefore, TiO_2-EPE/CA mat displayed very similar value of Young's modulus than TiO_2/CA mat despite the plasticising effect of PEO block. This behaviour can be related to a more homogeneous distribution of the nanoparticles along the fibre surface as concluded before from TEM measurement and achieved due to the self-assembly ability of the EPE triblock copolymer which is able to microphase separated from CA matrix during the electrospinning process.

Contact angle measurements

The digital images and WCA values are collected in Fig. S5. CA mat presented a WCA of $133° \pm 7°$, which is higher than those reported in the literature (Wang et al. 2015; Elsherbiny et al. 2022). Moreover, this WCA was 8% higher than that of CA mat

prepared in different electrospinning conditions (feed rate of 7 mL/h, 7 kV and −0.8 kV voltage and a distance of 12 cm), which displayed a 123° ± 5° value. This confirmed the strong influence of the electrospinning conditions on the designed mat properties. Taking this into account, in this work the electrospinning conditions that allow to achieve the highest hydrophobicity for CA mat were chosen for the preparation of all investigated mats.

The incorporation of sol–gel synthesised TiO_2 nanoparticles led to an increase of the hydrophobicity, increasing by 5% the WCA for TiO_2/CA mat (140° ± 6°), since this value was almost one for the superhydrophobic surfaces (very near to 150°) (Wang et al. 2022c). As previously reported, the hydrophobicity of surfaces is closely related to the surface energy and roughness of the material (Yang et al. 2021). As observed by SEM images, mats with sol–gel synthesised TiO_2 nanoparticles possessed a low fibre diameter and pore size and with high fibre density, leading to a higher hydrophobicity.

As shown in Table S3, there were differences in the WCA for CA and TiO_2/CA mats after the layer-by-layer peeling process. CA mat displayed a decrease of the WCA after peeling. For TiO_2/CA mat, after the first layer was taken off, the WCA remained constant. However, consecutive peeling led to a slight decrease of the WCA. Every time that a peeled layer is removed, the mat loses density and an increase in pore size is more likely, which facilitates the wettability of the water droplet and resulted in a decrease of the WCA.

Due to the hydrophilic nature of PEO blocks in EPE/CA and TiO_2-EPE/CA mats the water droplet was absorbed a priori the contact angle measurement.

Self-cleaning

The high hydrophobic character of CA and TiO_2/CA mats can endow them with self-cleaning ability. For CA mat, the surface deteriorated after the water droplet was poured on it, and residual chalk was clearly observed on its surface (Fig. 4). Moreover, after peeling process, some pink colour remained on the surface of this mat. On the contrary, the water droplet removed the chalk contaminant from the surface of TiO_2/CA mat, resulting in an almost clean and dry surface with only a few fibres impregnated with chalk powder. After the peeling process, the surface was completely clean.

Although the contact angle of EPE/CA and TiO_2-EPE/CA mats was not measured, a self-cleaning test attempt was carried out. EPE/CA mat did not present any self-cleaning ability, since the mat absorbed the water droplet and was not able to remove the chalk powder (Fig. S6). Additionally, peeling was more complicated. Therefore, this mat did not possess self-cleaning properties. Nevertheless, the addition of TiO_2 nanoparticles provided self-cleaning ability to TiO_2-EPE/CA mat. After pouring the water, the surface did not deteriorate as for CA mat, and although not all of the chalk powder could be removed as for TiO_2/CA mat, some of it was erased. Moreover, after peeling process, the surface was clean, but still somewhat wet due to the absorption of water by the EPE triblock copolymer with high PEO block content.

Here it can be concluded that the addition of sol–gel synthesised TiO_2 nanoparticles improved the hydrophobicity of mats regarding waterproof materials. This phenomenon is probably related to both the well-known self-cleaning properties of the TiO_2 nanoparticles and the change in the morphology (different fibre diameter and pore size and, as a consequence, the density of the mats) as observed by SEM and TEM images.

Solvent resistance

The solvent resistance of the fabricated mats was studied after immersion during 7 days in water, IPA, acetone and toluene (Fig. 5).

CA mat was deteriorated in water and some small fibres were detected, slightly clouding the solution. The water molecules, due to their high dipole moment (1.87) and polarity index (10.2), are very prone to form hydrogen bonds.

Consequently, they can weaken to some extent the intermolecular hydrogen bonds of CA itself for CA mat, resulting in the detaching of small fibres from the main mat. However, the mat did not dissolve because, as is well known, the CA molecules are strongly bound by a large number of hydrogen bonds that prevent the penetration of water (Alves et al. 2016; Rincón-Iglesias et al. 2019). Thus, the weight loss observed for CA mat (Table S4) was due to the separation of these fibres. On the contrary, CA mat

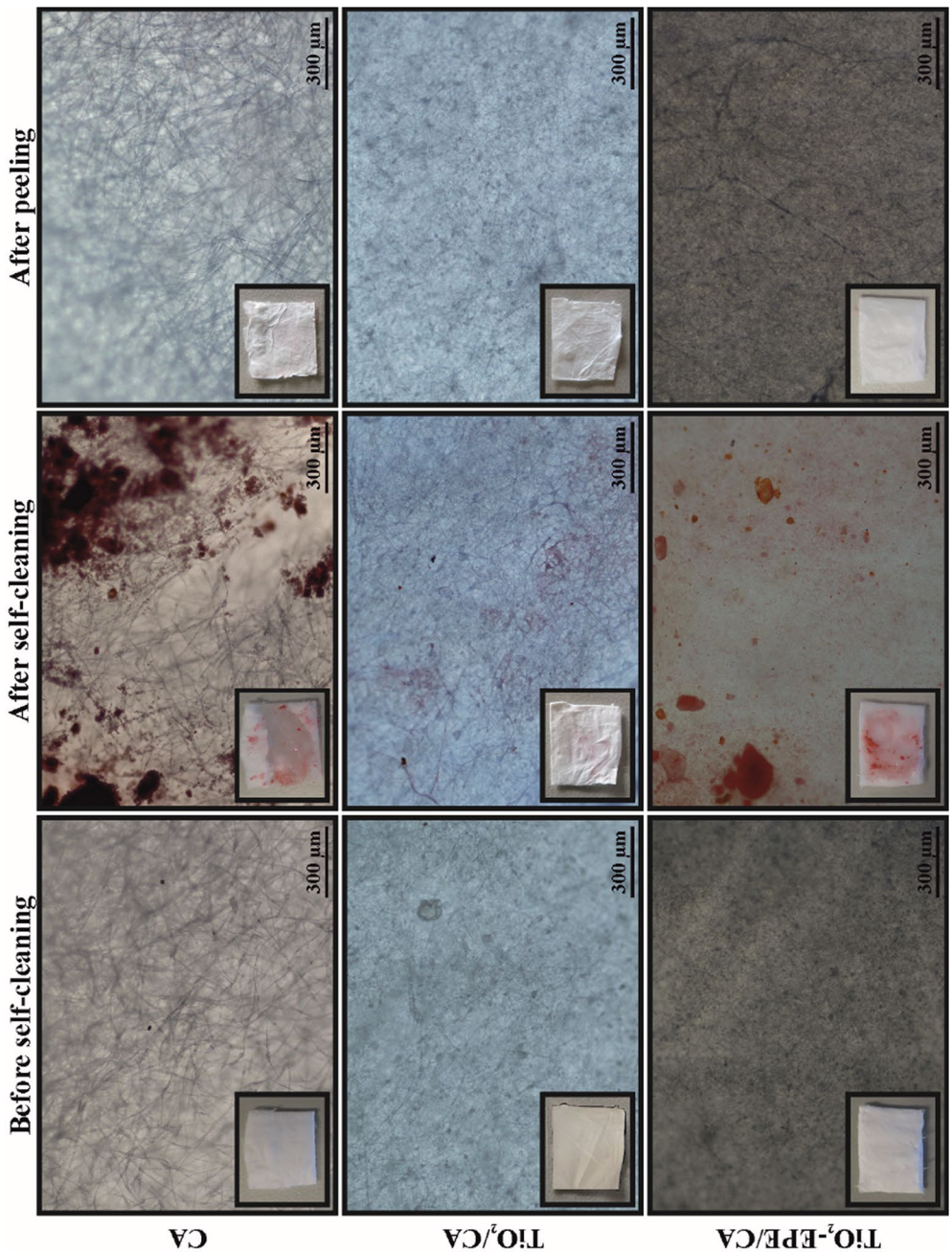

Fig. 4 OM micrograph and digital images (inset of each image) of fabricated mats before self-cleaning, after self-cleaning and after peeling

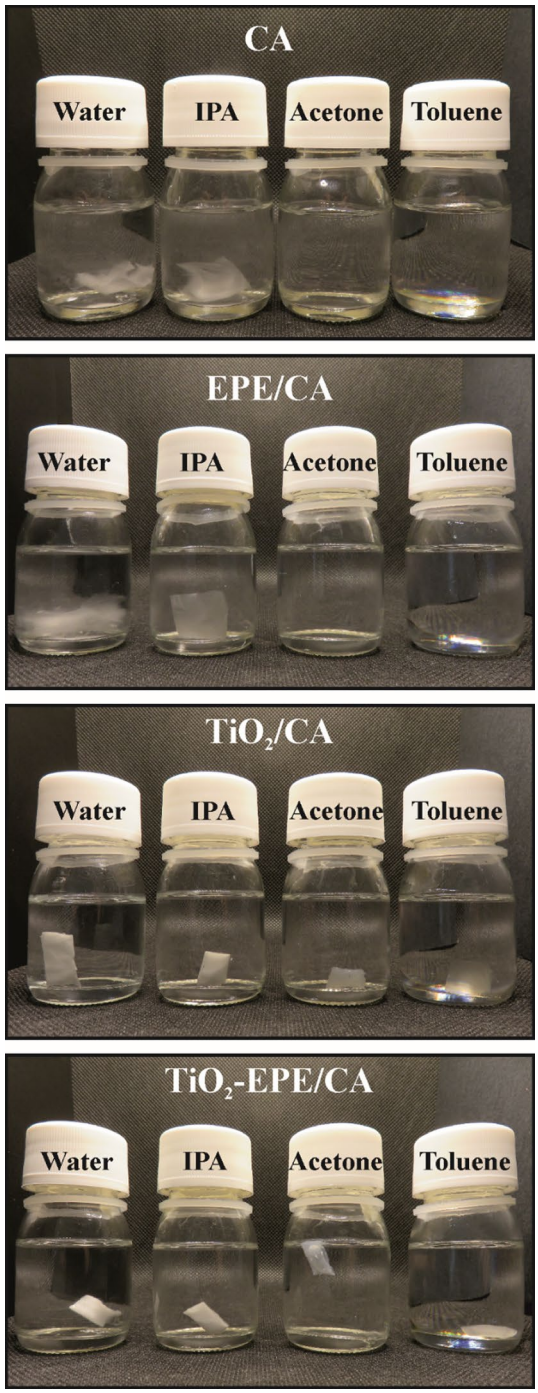

Fig. 5 Digital images of fabricated mats in different solvents after 7 days

integrity was better maintained in IPA and not as many fibres were seen in the solution. This minor difference can be ascribed to a lower dipole moment (1.66) and polarity index (3.9) of IPA if compared with water, which set the lower hydrogen bonding capacity of IPA. Additionally, as it is well known, CA mat was soluble in acetone. In the case of toluene, it turned transparent when immersed in the solvent, recovering its initial white colour after drying. This phenomenon is explained by taking into account the refractive index of CA mat and solvents. CA presented a value of 1.47 (Guo et al. 2021; Sultanova et al. 2009), whereas the solvents have a value of 1.33 for water, 1.38 for IPA, 1.36 for acetone and 1.49 for toluene (Akagi et al. 2012; Volk et al. 2005). Therefore, only toluene has a value similar to CA, which leads to similar refraction of light in both mediums resulting in the high transparency of CA mat in toluene. It is worth nothing that, the weight loss was very low, indicating the high stability of the CA mat in this solvent with low dipole moment (0.31) and polarity index (2.4).

As for CA, EPE/CA mat fibres were released after soaking in water and IPA, and they were completely dissolved in acetone. EPE/CA mat was also transparent in toluene since the refractive index of EPE was ~ 1.46. Moreover, it displayed higher weight loss than CA mat, probably due to the solubility of the EPE triblock copolymer in this solvent. Nevertheless, the TiO_2 nanoparticles provoked changes in the solvent resistance of the mats. In water, as well as in IPA and toluene, TiO_2/CA mat retained its mat integrated structure during all 7 days without any detaching, as well as preserving its characteristic white colour in both water and IPA. In toluene, the mat was transparent when immersed in the solvent, however, some opaque domains were distinguished. Those areas could correspond to TiO_2 nanoparticles, which have higher refractive index (2.5–2.9) than EPE and CA (Kischkat et al. 2021; Yovcheva et al. 2012). After drying it recovered its initial white colour, similar to CA and EPE/CA mats. Besides, the TiO_2/CA mat did not show weight loss in any of the three solvents. In the case of acetone, a 20% weight loss was observed, being this value very low if compared with the 100% weight loss for CA mat. This can be related to the fact that in this solution, CA fibres were coated by TiO_2 nanoparticles.

Thus, the addition of sol–gel synthesised TiO_2 nanoparticles prevented CA from being dissolved in acetone and enhanced the mat integrity in polar solvents such as water by preventing the formation

of hydrogen bonds between the solvent and the CA fibres. Obtained solubility results indicated that TiO_2 nanoparticles were well-attached to CA fibres, since they did not separate from the mat in the presence of solvent, contrary to neat sol–gel solution, in which the nanoparticles precipitated in it.

Similar behaviour was observed for TiO_2-EPE/CA mat, which stability was very similar in IPA and the weight loss in acetone and toluene was lower if compared with EPE/CA. Consequently, it can be concluded that there was a good compatibility between the components of this mat, as detected from DSC, and that sol–gel synthesised TiO_2 nanoparticles improved the solvent resistance of investigated mats.

Conclusions

Mats based on cellulose acetate (CA), poly (ethylene oxide-b-propylene oxide-b-ethylene oxide (EPE) and sol–gel synthesised TiO_2 nanoparticles were fabricated by the electrospinning process, being this process more effective for mats with EPE due to the higher spinnability of PEO block. The addition of 10 wt% TiO_2 nanoparticles led to mats with a whiter colour, as well as an easily detected micrometric multilayer structure and, as a consequence, a better layer-by-layer peeling ability. DSC results confirmed a partial miscibility of the components of the mats. High magnification SEM images confirmed the lack of macrophase separation of PPO block of EPE triblock copolymer in EPE/CA mat and no agglomeration of TiO_2 nanoparticles in TiO_2/CA and TiO_2-EPE/CA mats. SEM results also indicated a decrease in the fibre diameter and pore size when TiO_2 nanoparticles were added. Therefore, this led to increased mat hydrophobicity and improved their self-cleaning ability. These properties were better for TiO_2/CA than for TiO_2-EPE/CA, due to the absorption of water by the EPE triblock copolymer. On the other hand, TEM results proved that EPE triblock copolymer self-assembled during electrospinning process leading to microphase separation of PPO block of EPE triblock copolymer from the PEO block/CA matrix and formation of TiO_2 nanoparticles with the size of ~ 8 nm in diameter. The addition of TiO_2 nanoparticles also improved the mechanical properties, being the Young's modulus of TiO_2/CA and TiO_2-EPE/CA mats higher than CA and EPE/CA mats. In addition, the Young's modulus of TiO_2-EPE/CA mat was similar to that for TiO_2/CA mat despite the plasticising effect of PEO block. Thus, the nanostructuration of the fibres by self-assembly of EPE triblock copolymer can be responsible for a better distribution of TiO_2 nanoparticles. At the same time, the addition of sol–gel synthesised TiO_2 nanoparticles resulted in the improvement of the solvent resistance of these mats against water, IPA, acetone and toluene. In summary, the addition of EPE triblock copolymer allowed to achieve nanostructured mats even in presence of TiO_2 nanoparticles. Furthermore, the presence of TiO_2 nanoparticles resulted in significant improvement of Young's modulus, solvent stability and self-cleaning properties with a very easy layer-by-layer peeling process, which make them ideal as waterproof and disposable dressings.

Acknowledgments Financial support from Spanish Ministry of Science, Innovation and Universities and European Union (MICINN/FEDER and UE) in the frame of PGC2018-097699-B-I00 and PID2021-126417NB-I00 projects, and from the Basque Government for PIBA19-0044 and IT1690-22 projects are gratefully acknowledged. Moreover, Macrobehaviour-Mesostructure-Nanotechnology, Microscopy: Polymer Characterization Service and Analytical and High-Resolution Microscopy in Biomedicine SGIker units of UPV/EHU were also acknowledged. J.G.-H.-de-M. thanks Basque Government for PhD Fellowship (PRE_2021_2_0044).

Author contributions JG-H-d-M: Methodology, investigation, writing-original draft, visualization. JG: Conceptualization, methodology, resources, writing-review and editing, visualization, supervision. AT: Conceptualization, methodology, resources, writing-review and editing, visualization, supervision.

Funding Open Access funding provided thanks to the CRUE-CSIC agreement with Springer Nature. This work was founded by Spanish Ministry of Science, Innovation and Universities and European Union (MICINN/FEDER and UE) in the frame of PGC2018-097699-B-I00 and PID2021-126417NB-I00 projects, and by Basque Government in frame of PIBA19-0044. J.G.-H.-de-M. thanks Basque Government for PhD Fellowship (PRE_2021_2_0044).

Declarations

Conflict of interest The authors declare that they have no known competing financial interests or personal relationships that could have appeared to influence the work reported in this paper.

References

Aboamera NM, Mohamed A, Salama A, Osman TA, Khattab A (2019) Characterization and mechanical properties of electrospun cellulose acetate/graphene oxide composite nanofibers. Mech Adv Mater Struct 26:765–769. https://doi.org/10.1080/15376494.2017.1410914

Akagi M, Yanagida S, Yasumori A (2012) Fabrication of LSPR sensor using porous titania-glass composite loading Au nanoparticles by photocatalytic deposition method. Procedia Eng 36:154–159. https://doi.org/10.1016/j.proeng.2012.03.024

Alves L, Medronho B, Antunes FE, Topgaard D, Lindman B (2016) Dissolution state of cellulose in aqueous systems. 2. Acidic solvents. Carbohydr Polym 151:707–715. https://doi.org/10.1016/j.carbpol.2016.06.015

Angel N, Guo L, Yan F, Wang H, Kong L (2020) Effect of processing parameters on the electrospinning of cellulose acetate studied by response surface methodology. J Agric Food Res 2:100015. https://doi.org/10.1016/j.jafr.2019.100015

Angel N, Li S, Yan F, Kong L (2022) Recent advances in electrospinning of nanofibers from bio-based carbohydrate polymers and their applications. Trends Food Sci Technol 120:308–324. https://doi.org/10.1016/j.tifs.2022.01.003

Arrieta MP, Perdiguero M, Fiori S, Kenny JM, Peponi L (2020) Biodegradable electrospun PLA-PHB fibers plasticized with oligomeric lactic acid. Polym Degrad Stab 179:109226. https://doi.org/10.1016/j.polymdegradstab.2020.109226

Arumugam M, Murugesan B, Pandiyan N, Chinnalagu DK, Rangasamy G, Mahalingam S (2021) Electrospinning cellulose acetate/silk fibroin/Au–Ag hybrid composite nanofiber for enhanced biocidal activity against MCF-7 breast cancer cell. Mater Sci Eng C 123:112019. https://doi.org/10.1016/j.msec.2021.112019

Bazzi M, Shabani I, Mohandesi JA (2022) Enhanced mechanical properties and electrical conductivity of chitosan/polyvinyl alcohol electrospun nanofibers by incorporation of graphene nanoplatelets. J Mech Behav Biomed Mater 125:104975. https://doi.org/10.1016/j.jmbbm.2021.104975

Cai J, Chen J, Zhang Q, Lei M, He J, Xiao A, Ma C, Li S, Xiong H (2016) Well-aligned cellulose nanofiber-reinforced polyvinyl alcohol composite film: mechanical and optical properties. Carbohydr Polym 140:238–245. https://doi.org/10.1016/j.carbpol.2015.12.039

Can-Herrera LA, Oliva AI, Dzul-Cervantes MAA, Pacheco-Salazar OF, Cervantes-Uc JM (2021) Morphological and mechanical properties of electrospun polycaprolactone scaffolds: effect of applied voltage. Polymers 13:662. https://doi.org/10.3390/polym13040662

Cao J, Hasegawa T, Asakura Y, Sun P, Yang S, Li B, Cao W, Yin S (2022) Synthesis and color tuning of titanium oxide inorganic pigment by phase control and mixed-anion co-doping. Adv Powder Technol 33:103576. https://doi.org/10.1016/j.apt.2022.103576

Cerqueira DA, Filho GR, Asunçao RMM (2006) A new value for the heat of fusion of a perfect crystal of cellulose acetate. Polym Bull 56:475–484. https://doi.org/10.1007/s00289-006-0511-9

Chamankar N, Khajavi R, Yousefi AA, Rashidi A, Golestanifard F (2020) A flexible piezoelectric pressure sensor based on PVDF nanocomposite fibers doped with PZT particles for energy harvesting applications. Ceram Int 46:19669–19681. https://doi.org/10.1016/j.ceramint.2020.03.210

Chong WJ, Shen S, Li Y, Trinchi A, Pejak D, Kyratzis I, Sola A, Wen C (2022) Additive manufacturing of antibacterial PLA-ZnO nanocomposites: benefits, limitations and open challenges. J Mater Sci Technol 111:120–151. https://doi.org/10.1016/j.jmst.2021.09.039

de la Cruz LIS, Rodríguez FJM, Velasco-Santos C, Martínez-Hernández A, Gutiérrez-Sánchez M (2016) Hydrolytic degradation and morphological characterization of electrospun poly(glycolic acid) [PGA] thin films of different molecular weights containing TiO_2 nanoparticles. J Polym Res 23:113. https://doi.org/10.1007/s10965-016-1002-9

El-Aassar MR, El Fawal GF, El-Deeb NM, Hassan HS, Mo X (2016) Electrospun polyvinyl alcohol/Pluronic F127 blended nanofibers containing titanium dioxide for antibacterial wound dressing. Appl Biochem Biotechnol 178:1488–1502. https://doi.org/10.1007/s12010-015-1962-y

Elsherbiny DA, Abdelgawad AM, El-Naggar ME, Hemdane BA, Ghazanfari S, Jockenhövel S, Rojas OJ (2022) Bioactive tri-component nanofibers from cellulose acetate/lignin/N-vanillidene-phenylthiazole copper-(II) complex for potential diaper dermatitis control. Int J Biol Macromol 205:703–718. https://doi.org/10.1016/j.ijbiomac.2022.02.192

Gaan S, Rupper P, Salimova V, Heuberger M, Rabe S, Vogel F (2009) Thermal decomposition and burning behavior of cellulose treated with ethyl ester phosphoramidates: effect of alkyl substituent on nitrogen atom. Polym Degrad Stab 94:1125–1134. https://doi.org/10.1016/j.polymdegradstab.2009.03.017

Ghorani B, Russel SJ, Goswami P (2013) Controlled morphology and mechanical characterisation of electrospun cellulose acetate fibre webs. Int J Polym Sci 2013:256161. https://doi.org/10.1155/2013/256161

Goetz LA, Jalvo B, Rosal R, Mathew AP (2016) Superhydrophilic anti-fouling electrospun cellulose acetate membranes coated with chitin nanocrystals for

water filtration. J Membr Sci 510:238–248. https://doi.org/10.1016/j.memsci.2016.02.069

Gomez-Hermoso-de-Mendoza J, Barud HS, Gutierrez J, Tercjak A (2019) Flexible photochromic cellulose triacetate based bionanocomposites modified with sol–gel synthesized V_2O_5 nanoparticles. Carbohydr Polym 208:50–58. https://doi.org/10.1016/j.carbpol.2018.12.045

Gomez-Hermoso-de-Mendoza J, Gutierrez J, Tercjak A (2021) Comparative study of nano and macro mechanical properties of cellulose triacetate based nanocomposites by mean of quantitative nanomechanical mapping and mechanical testing. Compos Sci Technol 211:108851. https://doi.org/10.1016/j.compscitech.2021.108851

Gorbacheva SN, Yadykova AY, Ilyin SO (2021) Rheological and tribological properties of low-temperature greases based on cellulose acetate butyrate gel. Carbohydr Polym 272:118509. https://doi.org/10.1016/j.carbpol.2021.118509

Gosal K, Agatemor C, Špitálsky Z, Thomas S, Kny E (2019) Electrospinning tissue engineering and wound dressing scaffolds from polymer-titanium dioxide nanocomposites. Chem Eng J 358:1262–1278. https://doi.org/10.1016/j.cej.2018.10.117

Guo J, Zhang X, Tian J, Zhu W, Song J, Xiao H (2021) Evaluating the refractive index, thickness and porosity of ultrathin cellulose nanocrystal films with different polymorphs by SPR technique. Int J Biol Macromol 193:1209–1214. https://doi.org/10.1016/j.ijbiomac.2021.10.158

Gutierrez J, Tercjak A, Algar I, Retegi A, Mondragon I (2012) Conductive properties of TiO_2/bacterial cellulose hybrid fibres. J Colloid Interf Sci 377:88–93. https://doi.org/10.1016/j.jcis.2012.03.075

Gutierrez J, Fernandes SCM, Mondragon I, Tercjak A (2013) Multifunctional hybrid nanopapers based on bacterial cellulose and sol–gel synthesized titanium/vanadium oxide nanoparticles. Cellulose 20:1301–1311. https://doi.org/10.1007/s10570-013-9898-2

Gutierrez J, Carrasco-Hernandez S, Barud HS, Oliveira RL, Carvalho RA, Amaral AC, Tercjak A (2017) Transparent nanostructured cellulose acetate films based on the self assembly of PEO-b-PPO-b-PEO block copolymer. Carbohydr Polym 165:437–443. https://doi.org/10.1016/j.carbpol.2017.02.070

Kischkat J, Peters S, Gruska B, Semtsiv M, Chashnikova M, Klinkmüller M, Fedosenko O, Machulik S, Aleksandrova A, Monastyrski G, Flores Y, Masselink WT (2021) Mid-infrared optical properties of thin films of aluminum oxide, titanium dioxide, silicon dioxide, aluminum nitride, and silicon nitride. Appl Opt 51:6789–6798. https://doi.org/10.1364/AO.51.006789

Li B, Yang X (2020) Rutin-loaded cellulose acetate/poly(ethylene oxide) fiber membrane fabricated by electrospinning: a bioactive material. Mater Sci Eng C 109:110601. https://doi.org/10.1016/j.msec.2019.110601

Luraghi A, Peri F, Moroni L (2021) Electrospinning for drug delivery applications: a review. J Control Release 334:463–484. https://doi.org/10.1016/j.jconrel.2021.03.033

Mimura K, Moriya M, Sakamoto W, Yogo T (2010) Synthesis of $BaTiO_3$ nanoparticle/poly(2-hydroxyethyl methacrylate) hybrid nanofibers via electrospinning. Compos Sci Technol 70:492–497. https://doi.org/10.1016/j.compscitech.2009.11.026

Morselli D, Valentini P, Perotto G, Scarpellini A, Pompa PP, Athanassiou A, Fragouli D (2017) Thermally-induced in situ growth of ZnO nanoparticles in polymeric fibrous membranes. Compos Sci Technol 149:11–19. https://doi.org/10.1016/j.compscitech.2017.05.025

Motora KG, Wu CM, Xu TZ, Chala TF, Lai CC (2020) Photocatalytic, antibacterial, and deodorization activity of recycled triacetate cellulose nanocomposites. Mater Chem Phys 240:122260. https://doi.org/10.1016/j.matchemphys.2019.122260

Nair SS, Mathew AP (2017) Porous composite membranes based on cellulose acetate and cellulose nanocrystals via electrospinning and electrospraying. Carbohydr Polym 175:149–157. https://doi.org/10.1016/j.carbpol.2017.07.048

Nandagopal S, Augustine R, George SC, Jayachandran VP, Kalarikkal N, Thomas S (2016) Gentamicin loaded electrospun poly(ε-caprolactone)/TiO_2 nanocomposite membranes with antibacterial property against Methicillin resistant *Staphylococus aureus* (MRSA). Polym Plast Technol Eng 55:1785–1796. https://doi.org/10.1080/03602559.2016.1171877

Neppalli R, Causin V, Benetti EM, Ray SS, Esposito A, Wanjale S, Birajdar M, Saiter JM, Marigo A (2014) Polystyrene/TiO_2 composite electrospun fibers as fillers for poly(butylene succinate-co-adipate): structure, morphology and properties. Eur Polym J 50:78–86. https://doi.org/10.1016/j.eurpolymj.2013.11.002

Passaro J, Imparato C, Parida D, Bifulco A, Branda F, Aronne A (2022) Electrospinning of PVP-based ternary composites containing SiO_2 nanoparticles and hybrid TiO_2 microparticles with adsorbed superoxide radicals. Compos B Eng 238:109874. https://doi.org/10.1016/j.compositesb.2022.109874

Rincón-Iglesias M, Lizundia E, Lanceros-Méndez S (2019) Water-soluble cellulose derivatives as suitable matrices for multifunctional materials. Biomacromol 20:2786–2795. https://doi.org/10.1021/acs.biomac.9b00574

Rodríguez-Tobías H, Morales G, Grande D (2019) Comprehensive review on electrospinning techniques as versatile approaches toward antimicrobial biopolymeric composite fibers. Mater Sci Eng C 101:306–322. https://doi.org/10.1016/j.msec.2019.03.099

Santamaria-Echart A, Ugarte L, Gonzalez K, Martin L, Irusta L, Gonzalez A, Corcuera MA, Eceiza A (2017) The role of cellulose nanocrystals incorporation route in water borne polyurethane for preparation of electrospun nanocomposites mats. Carbohydr Polym 166:146–155. https://doi.org/10.1016/j.carbpol.2017.02.073

Sinha R, Janaswamy S, Prasad A (2020) Enhancing mechanical properties of electrospun cellulose acetate fiber mat upon potassium chloride exposure. Materialia 14:100881. https://doi.org/10.1016/j.mtla.2020.100881

Sultanova N, Kasarova S, Nikolov I (2009) Dispersion properties of optical polymers. Acta Phys Pol 116:585–587. https://doi.org/10.12693/APhysPolA.116.585

Tian L, Zi-Qiang S, Jian-Quan W, Mu-Jia G (2015) Fabrication of hydroxyapatite nanoparticles decorated cellulose triacetate nanofibers for protein adsorption by coaxial electrospinning. Chem Eng J 260:818–825. https://doi.org/10.1016/j.cej.2014.09.004

Toniatto TV, Rodrigues BVM, Marsi TCO, Ricci R, Marciano FR, Webster TJ, Lobo AO (2017) Nanostructured poly (lactic acid) electrospun fiber with high loadings of TiO_2 nanoparticles: insights into bactericidal activity and cell viability. Mater Sci Eng C. https://doi.org/10.1016/j.msec.2016.10.026

Tsioptsiasa C, Sakellarioua KG, Tsivintzelis I, Papadopouloub L, Panayiotoua C (2010) Preparation and characterization of cellulose acetate-Fe_2O_3 composite nanofibrous materials. Carbohydr Polym 81:925–930. https://doi.org/10.1016/j.carbpol.2010.04.005

Vahabi H, Wu H, Saeb MR, Koo JH, Ramakrishna S (2021) Electrospinning for developing flame retardant polymer materials: current status and future perspectives. Polymer 217:123466. https://doi.org/10.1016/j.polymer.2021.123466

Volk J, Le Grand T, Bársony I, Gombköto J, Ramsden JJ (2005) Porous silicon multilayer stack for sensitive refractive index determination of pure solvents. J Phys D 38:1313–1317. https://doi.org/10.1088/0022-3727/38/8/032

Wable V, Biswas PK, Moheimani R, Aliahmad N, Omole P, Siegel AP, Agarwal M, Dalir H (2021) Engineering the electrospinning of MWCNTs/epoxy nanofiber scaffolds to enhance physical and mechanical properties of CFRPs. Compos Sci Technol 213:108941. https://doi.org/10.1016/j.compscitech.2021.108941

Wang SD, Ma Q, Liu H, Wang K, Ling LZ, Zhang KQ (2015) Robust electrospinning cellulose acetate@TiO_2 ultrafine fibers for dyeing water treatment by photocatalytic reactions. RSC Adv 5:40521. https://doi.org/10.1039/C5RA03797B

Wang D, Yue Y, Wang Q, Cheng W, Han G (2020) Preparation of cellulose acetate-polyacrylonitrile composite nanofibers by multi-fluid mixing electrospinning method: morphology, wettability, and mechanical properties. Appl Surf Sci 510:145462. https://doi.org/10.1016/j.apsusc.2020.145462

Wang F, Liu K, Xi Y, Li Z (2022a) One-step electrospinning PCL/ph-LPSQ nanofibrous membrane with excellent self-cleaning and oil–water separation performance. Polymer 249:124858. https://doi.org/10.1016/j.polymer.2022.124858

Wang K, Yu S, Li W, Song Y, Gong P, Zhang M, Li H, Sun D, Yang X, Wang X (2022b) Superhydrophobic and photocatalytic synergistic self-cleaning ZnS coating. Appl Surf Sci 595:153565. https://doi.org/10.1016/j.apsusc.2022.153565

Wang X, Deng M, Zhao Z, Zhang Q, Wang Y (2022c) Synthesis of super-hydrophobic CuO/ZnO layered composite nano-photocatalyst. Mater Chem Phys 276:125305. https://doi.org/10.1016/j.matchemphys.2021.125305

Yang J, Wang R, Long F, Zhang X, Liu J, Hu W, Liu L (2021) New perspectives on structural parameters and hydrophobic model inspired by a superhydrophobic Cu cone-flower coating. Mater Des 206:109827. https://doi.org/10.1016/j.matdes.2021.109827

Yoon YI, Moon HS, Lyoo WS, Lee TS, Pak WH (2009) Superhydrophobicity of cellulose triacetate fibrous mats produced by electrospinning and plasma treatment. Carbohydr Polym 75:246–250. https://doi.org/10.1016/j.carbpol.2008.07.015

Yovcheva T, Vlaeva I, Bodurov I, Dragostinova V, Sainov S (2012) Refractive index investigation of poly(vinyl alcohol) films with TiO_2 nanoparticle inclusions. Appl Opt 52:7771–7775. https://doi.org/10.1364/AO.51.007771

Zeng J, Liu S, Cai J, Zhang L (2010) TiO_2 immobilized in cellulose matrix for photocatalytic degradation of phenol under weak UV light irradiation. J Phys Chem C 114:7806–7811. https://doi.org/10.1021/jp1005617

Zhang Y, Zhang C, Liu K, Zhu X, Liu F, Ge X (2018) Biologically synthesized titanium oxide nanostructures combined with morphogenetic protein as wound healing agent in the femoral fracture after surgery. J Photochem Photobiol B 182:35–41. https://doi.org/10.1016/j.jphotobiol.2018.03.005

Zhang H, Zhu H, Xu C, Li Y, Liu Q, Wang S, Yan S (2022) Effect of nanoparticle size on the mechanical properties of polymer nanocomposites. Polymer 252:124944. https://doi.org/10.1016/j.polymer.2022.124944

Zheng S, Ai S, Guo Q (2003) Poly(hydroxyether of phenolphthalein) and its blends with poly(ethylene oxide). J Polym Sci Part B Polym Phys 41:466–475. https://doi.org/10.1002/polb.10392

Zhou H, Tong H, Lu J, Cheng Y, Qian F, Tao Y, Wang H (2021) Preparation of bio-based cellulose acetate/chitosan composite film with oxygen and water resistant properties. Carbohydr Polym 270:118381. https://doi.org/10.1016/j.carbpol.2021.118381